Cell Communication and Signaling

RESEARCH

Open Access

A non-catalytic role of IPMK is required for PLCγ1 activation in T cell receptor signaling by stabilizing the PLCγ1-Sam68 complex

Sehoon Hong[1], Kyurae Kim[2], Young-Ri Shim[2], Jiyeon Park[1], Sung Eun Choi[2], Hyungyu Min[3], Seulgi Lee[1], Ji-Joon Song[1], Suk-Jo Kang[1], Won-Il Jeong[2], Rho Hyun Seong[3] and Seyun Kim[1,4,5*]

Abstract

Background Phospholipase C gamma 1 (PLCγ1) is an important mediator of the T cell receptor (TCR) and growth factor signaling. PLCγ1 is activated by Src family kinases (SFKs) and produces inositol 1,4,5-triphosphate ($InsP_3$) from phosphatidylinositol 4,5-bisphosphate (PIP_2). Inositol polyphosphate multikinase (IPMK) is a pleiotropic enzyme with broad substrate specificity and non-catalytic activities that mediate various functional protein-protein interactions. Therefore, IPMK plays critical functions in key biological events such as cell growth. However, the contribution of IPMK to the activation of PLCγ1 in TCR signaling remains mostly unelucidated. The current study aimed to elucidate the functions of IPMK in TCR signaling and to uncover the mode of IPMK-mediated signaling action in PLCγ1 activation.

Methods Concanavalin A (ConA)-induced acute hepatitis model was established in $CD4^+$ T cell-specific IPMK knockout mice ($IPMK^{\Delta CD4}$). Histological analysis was performed to assess hepatic injury. Primary cultures of naïve $CD4^+$ T cells were used to uncover the role of mechanisms of IPMK in vitro. Western blot analysis, quantitative real-time PCR, and flow cytometry were performed to analyze the TCR-stimulation-induced PLCγ1 activation and the downstream signaling pathway in naïve $CD4^+$ T cells. Yeast two-hybrid screening and co-immunoprecipitation were conducted to identify the IPMK-binding proteins and protein complexes.

Results $IPMK^{\Delta CD4}$ mice showed alleviated ConA-induced acute hepatitis. $CD4^+$ helper T cells in these mice showed reduced PLCγ1 Y783 phosphorylation, which subsequently dampens calcium signaling and IL-2 production. IPMK was found to contribute to PLCγ1 activation via the direct binding of IPMK to Src-associated substrate during mitosis of 68 kDa (Sam68). Mechanistically, IPMK stabilizes the interaction between Sam68 and to PLCγ1, thereby promoting PLCγ1 phosphorylation. Interfering this IPMK-Sam68 binding interaction with IPMK dominant-negative peptides impaired PLCγ1 phosphorylation.

Conclusions Our results demonstrate that IPMK non-catalytically promotes PLCγ1 phosphorylation by stabilizing the PLCγ1–Sam68 complex. Targeting IPMK in $CD4^+$ T cells may be a promising strategy for managing immune diseases caused by excessive stimulation of TCR.

Keywords Inositol polyphosphate multikinase, Phospholipase C gamma 1, Sam68, T cell receptor, Hepatitis

*Correspondence:
Seyun Kim
seyunkim@kaist.ac.kr

Full list of author information is available at the end of the article

Introduction

IPMK is an enzyme that catalyzes the production of inositol polyphosphates (InsPs) and phosphatidylinositol 3,4,5-trisphosphate (PIP_3) [1, 2]. Specifically, the activation of the phospholipase C (PLC) product, inositol 1,4,5-trisphosphate ($InsP_3$), mediated by the 3- and 6-kinase activities of IPMK, yields inositol 1,3,4,5-tetrakisphosphate (Ins (1,3,4,5) P_4) and 1,4,5,6-tetrakisphosphate (Ins (1,4,5,6) P_4) [2]. Recent studies have highlighted the key roles of IPMK in immune cells [3–6]. IPMK-mediated production of $InsP_6$ in B cells is required for B cell receptor activation via Bruton's tyrosine kinase (Btk) [5]. IPMK depletion in regulatory T (Treg) cells results in reduced Ins(1,3,4,5)P_4, which leads to impaired Treg differentiation via reduced store-operated Ca^{2+} entry [6]. Furthermore, the non-catalytic actions of IPMK broaden the enzyme's signaling repertoire by directly interacting with key signaling molecules, such as SWI/SNF, p53, serum response factor (SRF), mechanistic target of rapamycin (mTOR), adenosine 5′-monophosphate–activated protein kinase (AMPK), and tumor necrosis factor receptor–associated factor 6 (TRAF6) [3, 7–11].

PLC yields the intracellular messengers of inositol $InsP_3$ and diacylglycerol (DAG) by catalyzing the hydrolysis of phosphatidylinositol 4,5-bisphosphate (PIP_2). Among the various PLC isoforms, PLC gamma 1 (PLCγ1) has particularly unique domain structures that harbor the Src homology 2 (SH2) and SH3 domains between the X and Y region [12]. Activation of PLCγ1 is a critical event that involves the phosphorylation of target proteins by non-receptor tyrosine kinases, such as Src family kinases (SFKs) and interleukin-2-inducible T-cell kinase (Itk) [12, 13]. Indeed, SFK-mediated phosphorylation of tyrosine 783 (Y783) in PLCγ1 is essential for stimulating its activities [14–16].

T cell activation is initiated in response to the antigen binding to the T cell receptor (TCR), triggering an adaptive immune response that eliminates pathogens [17, 18]. In this stimulation, PLCγ1 serves as the main effector of the TCR signaling cascade in $CD4^+$ helper T (Th) cells [19]. The activation of PLCγ1 produces $InsP_3$ and DAG, which are responsible for increasing the cytosolic Ca^{2+} levels and for activating nuclear factor of activated T cells (NFAT) and protein kinase C theta (PKCθ) [20]. Subsequently, this activates NF-κB, which results in the production of various cytokines, T cell proliferation, and the activation of the T cell effector functions. Despite recent advancements in TCR signaling research, our current understanding of the biochemical basis of PLCγ1 Y783 phosphorylation remains incomplete. In particular, little is known about the upstream events of this process, including how specific SFKs are engaged by PLCγ1 to initiate its phosphorylation and functional activation.

PLCγ1 phosphorylation involves a couple of extensive protein-protein interactions among various TCR signaling factors [21–24]. In particular, Src-associated substrate during mitosis of 68 kDa (Sam68) has been implicated to play an important role in PLCγ1 signaling [25, 26]. Sam68, also known as KH domain containing RNA binding signal transduction associated 1 (KHDRBS1), is a member of the signal transduction and activation of the RNA (STAR) family, which controls RNA alternative splicing [27, 28]. In response to TCR activation and independent of its RNA metabolism, SFKs (e.g., Fyn) phosphorylate Sam68 in the cytosol to form a signalosome with various signaling proteins, including Grb2, p120GAP, Cbl, and PLCγ1 [29–33]. Despite previous findings that propose the importance of Sam68 in TCR signaling, the mechanism(s) underlying Sam68-mediated PLCγ1 activation is not fully understood.

Here, we report that the deletion of IPMK in $CD4^+$ T cells diminishes PLCγ1 signaling and further ameliorates acute T cell activation-induced hepatic injury in vivo. Additionally, we identify binding between IPMK and Sam68, which is a critical event in the promotion of SFK-mediated PLCγ1 phosphorylation. Our work expands the traditional view that IPMK functions as an InsP kinase acting downstream of PLCγ1; instead, IPMK was found to play an upstream role in mediating PLCγ1 activation by stabilizing the Sam68–PLCγ1 complex.

Methods

Animal experiments

Animal protocols were performed in accordance with approved guidelines by the KAIST Animal Care and Use Committee (KAIST, KA2018-52). All mice were bred and housed under specific pathogen-free conditions in a 12-hour light–dark cycle. They received food and water *ad libitum*. CD4-Cre mice and *Ipmk*-floxed mice ($IPMK^{f/f}$), who exhibit C57BL/6 backgrounds, were used to generate CD4 helper T cell-specific IPMK knockout mice ($IPMK^{\Delta CD4}$) [34]. Male and female mice aged 8–10 weeks old were used for the experiments. Each mice-related experiment used littermates.

Induction of ConA-induced hepatitis

To induce acute hepatitis with T cell activation, PBS or concanavalin A (Sigma-Aldrich, St.Louis, MO) was administered intravenously (IV) via the lateral tail veins to mice weighing 24–26 g at a dose of 12 mg/kg. Serum and livers were obtained from the mice 12 h after the Con A injection. Serum alanine aminotransferase (ALT) and aspartate aminotransferase (AST) were measured using VetTest® Chemistry Analyzer and Catalyst One Chemistry Analyser (IDEXX Laboratory Inc., Westbrook, ME, USA). Liver mononuclear cells (MNCs) were isolated from liver tissues by grinding on a 70 mm

strainer and centrifuging twice at 50 x g for 5 min. After the supernatant was pelleted (650 x g for 10 min), they were purified using 40% Percoll gradient medium (GE Healthcare; 1,800 x g for 20 minnutes), and RBS lysis buffer (BioLegend).

Histological analysis

Mouse livers were fixed with 10% neutral buffered formalin (Sigma-Aldrich) and embedded in paraffin for histological analysis. Following deparaffinization and rehydration, the sectioned tissues (4 μm thickness) were stained with hematoxylin and eosin (H&E). For apoptotic cell staining, terminal deoxynucleotidyl transferase dUTP nick end labeling (TUNEL) staining was performed in liver tissues, in accordance with the data protocol provided with the In Situ Cell Death Detection Kit, Fluorescein (Roche).

Cell culture and transfection

Mouse embryonic fibroblasts (MEFs), HEK293T, and NIH3T3 cells were maintained in the following reagents: high-glucose Dulbecco's modified Eagle's medium (DMEM) (Biowest); 10% fetal bovine serum (FBS) (Atlas Biologicals); 100 mg/mL penicillin/streptomycin (Welgene). MEFs were obtained from $IPMK^{f/f}UBC^{Cre-ERT2}$ mice and they were immortalized by transfecting an SV40 large T-antigen plasmid. To deplete IPMK, 1 μM 4-hydroxytamoxifen was treated with MEFs for 48 h. Thereafter, 10 ng/mL PDGF was administered into cells for each reagent-suitable time and condition (serum starvation for 12 h), when required.

For transient transfection, we used several reagents: jetPRIME reagent (Polyplus) was used for DNA plasmid overexpression in HEK293T cells, following the manufacturer's protocol. Lipofectamine LTX (Invitrogen) was used for DNA plasmid overexpression in NIH3T3 cells, following the manufacturer's protocol. NIH3T3 cells were transfected siRNA using Lipofectamine RNAiMAX (Invitrogen). The list of siRNAs used for knockdown is provided as follows (Bioneer): IPMK (Sense: 5′-CAGAG AGGUCCUAGUUAAUUUCA-3′, Antisense: 5′-AGUG AAAUUAACUAGGACCUCUCUGUU-3′).

In vitro $CD4^+$ helper T cell differentiation, proliferation, and TCR stimulation

Naïve $CD4^+$ T cells were isolated from the mouse spleen and inguinal/mesenteric lymph nodes by MACS naïve $CD4^+$ T cell isolation kit, mouse (Miltenyi Biotec) or MagniSort mouse CD4 naïve T cell enrichment kit (Invitrogen), following the manufacturer's protocols. Isolated $CD4^+$ T cells were plated on plates coated with 10 μg/mL anti-CD3 (16-0031-85, eBioscience) and 10 μg/mL anti-CD28 (16-0281-86, eBioscience) and 55 μM β-mercaptoethanol (Gibco) was also added to the media. The cells were incubated under Th0 cells using 5 μg/mL anti-IFN-γ (16-7311-85) and 5 μg/mL anti-IL-4 (16-7041-85) (eBioscience) in RPMI 1640 medium (Welgene). To trace cell proliferation, the CellTrace™ Carboxyfluorescein succinimidyl ester (CFSE) proliferation kit was used following the manufacturer's instructions (C34554, Invitrogen).

For TCR signaling stimulation, cells were first stabilized in RPMI 1640 medium at 37 °C for 10 min. Naïve $CD4^+$ T cells were incubated with 5 μg/mL anti-CD3 antibody and 2 μg/mL anti-CD28 antibodies in cold PBS at 4 °C for 20 min. Subsequently, 20 μg/mL anti-Armenian hamster IgG secondary antibody (Jackson ImmunoResearch Laboratory) was added to the RPMI 1640 medium and the cells were treated for either 3–10 min in a 37 °C heat block, after which the medium was rapidly replaced with cold PBS. Additionally, 1 μM PTD and PTD_93–126 (synthesized at Peptron, Daejeon, Korea) were transduced into stabilized naïve $CD4^+$ T cells prior to TCR stimulation in RPMI 1640 at 37 °C for one hour. For ConA-induced TCR signaling stimulation, 5 μg/mL ConA was used in place of antibody-induced TCR stimulation and applied for either 15–30 min.

Plasmid construction

The full-length Sam68 pCMV-GST and fragments were constructed from pcDNA3.0 HA-Sam68 WT DNA plasmid (Addgene) with a pCMV-GST vector. Full-length IPMK pCMV-GST and fragments were constructed as described previously [3, 11]. A MIGR1-Flag-IPMK-DN DNA plasmid was constructed in a MIGR1 vector, which was a gift from Dr. Rho Hyun Seong. LentiCRISPRv2 puro sgIPMK DNA plasmids were also constructed following a previous protocol from Zhang's Laboratory (GeCKO, Addgene) using *Ipmk* or *Khdrbs1* guided RNA, recommended from CHOPCHOP (https://chopchop.cbu.uib.no) (sgIPMK_1: 5'-AGGCCGTCCGCATCCGT CAG-3'; sgIPMK_2: 5'-GGACCAGACGCCGTAGTAT T-3'; sgSam68_1: 5'-TACGCAGAACAAAGTTACGA-3'; sgSam68_2: 5'-AGACGGCGTCTGACGCACCG-3').

Virus production and transduction of cells

Viruses were generated in HEK293T cells by transfecting the lentiviral DNA plasmid (lentiCRISPRv2 puro vector) with pMD2G and psPAX2.0, or the retroviral DNA plasmid with pCL-Eco viral packaging vector. Viral supernatants were collected 48 h after transfection and used to transduce target cells with 8 μg/mL polybrene for 24 h, after which the medium was replaced with fresh medium. The lentiCRISPRv2 virus-transduced cells were selected with 2 mg/mL puromycin (Gibco) after 48 h of cell incubation. Additionally, retroviruses were transduced into naïve $CD4^+$ T cells, which already incubated for one day on anti-CD3/anti-CD28 antibodies-coated plates. The

medium was replaced with Th0 cell-conditioned media after 24 h of transduction, and cells were incubated for an additional 72 h either on anti-CD3/anti-CD28 antibody-coated plates or 20 ng/ml IL-2 (Peprotech).

Yeast two-hybrid screening

The data from the yeast two-hybrid screening are the same as those presented by Beon, Han et al. [10]. The AH109 Saccharomyces cerevisiae strain (Clontech) underwent co-transformation with the full-length pGBKT7-hIPMK DNA plasmid, harboring the GAL4-DNA binding domain (BD), and a human brain cDNA activation domain (AD) library (Clontech). Selection markers included two different reporter genes, HIS3 and ADE2. Transformants were plated on a selection medium lacking leucine, tryptophan, and adenine or histidine (SD-LWA and SD-LWH). Candidate prey genes from the library were either amplified via PCR or transformed into *E. coli* to validate interactions, then reintroduced into the AH1009 yeast strain alongside the IPMK bait plasmid. All procedures for yeast two-hybrid screening were outsourced to Panbionet (Pohang, South Korea, http://panbionet.com).

SDS-PAGE and immunoblotting

For immunoblot analysis, cells were washed with PBS and lysed in lysis buffer consisting of 40 mM (pH 7.4) Tris–HCl, 1 mM EDTA, 1.5 mM sodium orthovanadate, 1% NP-40, 50 mM sodium fluoride, 10 mM sodium pyrophosphate, 200 mM NaCl, and protease inhibitor cocktail (Roche). Protein concentrations were determined by Bradford protein assay (Bio-rad) and the subsequent protein lysates were boiled at 95 °C for 5 min with SDS sample loading buffer (25% glycerol, 0.1% bromophenol blue, 60 mM Tris–HCl, 2% SDS, and 14.4 mM β-mercaptoethanol). A total of 10–20 μg of protein lysates was electrophoresed on SDS-PAGE gels and the separated proteins were transferred onto a nitrocellulose membrane. After blocking with 5% skim milk in Tris-buffered saline (TBS-T, 0.1% Tween-20), the membranes were blotted with primary antibodies and HRP-conjugated secondary antibodies. Antibodies against the following proteins were obtained from the indicated sources: Flag (F1804), Tubulin (T5109) (Sigma Aldrich); Sam68 (sc-1238), normal rabbit IgG (sc-2027), GAPDH (sc-32233), LAT (sc-53550) (Santa Cruz Biotechnology); HA (MMS-101R, Biolegend); GST (2622), β-actin (4970), phospho-PLCγ1 (Tyr783) (2821), PLCγ1 (5690), phospho-Src family (Tyr416) (6943), Src (2108), phospho-PKCθ (Thr538) (9377), PKCθ (13643) (Cell Signaling Technology). IPMK (NBP1-32250, Novus Biologicals).

Immunoprecipitation and GST pull-down assays

For immunoprecipitation, 160 μg to 2 mg of total protein lysates were incubated with 0.5 μg to 2 μg of primary antibodies or 10 μL net volume of anti-Flag M2 beads (Millipore) overnight with rotation at 4 °C. A total net volume of 10 μL of TrueBlot beads (Rockland Immunochemicals) was added to lysates with antibodies and incubated for additional 2 h, then, the samples were washed three times with lysis buffer and boiled at 95 °C for 5 min with 10 μL of 1 M DTT and 2x Laemmli sample loading buffer (100 mM Tris–HCl, 20% glycerol, 4% SDS, 28.8 mM β-mercaptoethanol, and 0.05% bromophenol blue).

For the GST pull-down assay, 10 μL net volume of glutathione agarose beads (Incopharm) were added to 1.5 mg to 2 mg of total protein lysates and incubated overnight at 4 °C with rotation, then, the samples were washed three times with lysis buffer and boiled at 95 °C for 5 min with SDS sample loading buffer.

In vitro binding assay

For the in vitro binding assay, recombinant human IPMK protein was purified, as described previously [35]. 500 ng of Flag-Sam68 purified protein (TP300263, OriGene) was incubated with 10 μL net volume of anti-Flag M2 beads in 0.1 M NaCl TGEM buffer (20 mM Tris–HCl, 20% glycerol, 1 mM EDTA, 5 mM $MgCl_2$, 1 mM DTT, 0.2 mM PMSF, and 100 mM NaCl) for 2 h at 4 °C with rotation. Then, the samples were washed with 0.5 M NaCl TGEM buffer and 0.1 M NaCl TGEM buffer, twice each. Afterward, 500 ng human IPMK purified protein was added to the samples with 0.1 M NaCl TGEM buffer and incubated at 4 °C with rotation for an hour. Finally, the samples were washed three times with 0.1 M NaCl TGEM buffer and boiled at 95 °C for 5 min with 10 μL of 1 M DTT and 2x Laemmli sample loading buffer.

In vitro kinase assay

In vitro kinase assay was conducted using PLCγ1, Sam68, Src, and IPMK purified proteins, according to a previously described protocol by Jones N. P. et al. and Rodriguez R. et al. [36, 37]. A total of 100 ng Flag-PLCγ1 (TP316448, OriGene), 150 ng Flag-Sam68 (TP300263, OriGene), and 150 ng GST-Src (10755-H20B, Sino Biological) were incubated at 37 °C for 10 min in kinase assay buffer (50 mM Tris pH 8, 0.2 mM $MnCl_2$, 2 mM $MgCl_2$, 2 mM DTT, and 0.02% TritonX-100) to form a complex. Then, 150 ng His-human IPMK protein, 50 μM ATP, and 1 mM Na_3VO_4 was added in an iced-cold protein mixture, or kinase assay buffer was added alongside 50 μM ATP, and 1 mM Na_3VO_4, and used as the control. Kinase assay was incubated at 37 °C for 20 min. Samples were boiled at 95 °C for 5 min with SDS sample loading buffer.

RNA isolation and RT-qPCR

RNA preparation and RT-qPCR protocols have been described previously [3]. Briefly, total RNA was isolated from cells using TRIzol reagent (Molecular Research Center), according to the manufacturer's protocol. A total of 1 μg of total RNA was used for the synthesis of first-strand cDNA by Superscript III reverse transcriptase (enzynomics). Quantitative real-time PCR analysis was performed using the SYBR Green master mix (Toyobo) and the Step One Plus Real-Time PCR system (Applied Biosystems). The primer sequences for RT-qPCR were as follows: *Actb* (forward: 5'-GTGGCATCCATGAAACTACA-3'; reverse: 5'-CTCATCGTACTCCTGCTTGC-3'), *Ipmk* (forward: 5'-CCAAAAT-ATTATGGCATCTG-3'; reverse: 5'-TATCTTTACATCCATTATAC-3'), *Il2* (forward: 5'-AACCTGAAACTCCCCAGGAT-3'; reverse: 5'-TCATCGAATTGGCACTCAAA-3').

Flow cytometry

To assess cytokine production in $CD4^+$ T cells, their stimulation was induced using 50 ng/mL PMA (Calbiochem) and 500 ng/mL ionomycin (Sigma Aldrich) with brefeldin A (Invitrogen; 1:1000) for 3 h. Fixable Viability Dye (65-0866-14, eBioscience) was administered to $CD4^+$ T cells for 30 min to exclude any dead cells. Next, fluorescent-conjugated antibodies were added for 20 min to stain the CD4 cell surface markers. Then, $CD4^+$ T cells were fixed and permeabilized using each previously described step-appropriate buffer (Invitrogen). Finally, $CD4^+$ T cells were incubated with fluorescent-conjugated antibodies for 30 min to stain IL-2 cytokines. Flow cytometry was performed by LSRII Fortessa (BD) and data were analyzed using the FlowJo software (FlowJo). The fluorescent-conjugated antibodies used to detect cell surface markers or cytokines were as follows: anti-mouse CD4 eFluor450 (48-0042-82), anti-mouse CD44 APC eFluor780 (47-0441-82), anti-mouse CD25 PE (12-0251-82), anti-mouse TCRβ (11-5961-82), anti-mouse IL-2 APC (17-7021-82), anti-mouse IFN gamma PE (12-7311-82), anti-mouse IL-4 (12-7041-82), anti-mouse IL-17 A PE-Cyanine7 (25-7177-82, eBioscience); and anti-mouse CD69 Alexa Fluor® 700 (561238), anti-mouse TNF PE (561063, BD Biosciences); phospho-PLCγ1 (Tyr783) Alexa Fluor® 647 (88717, Cell Signaling Technology).

Calcium flux measurement

Calcium flux was measured in naïve $CD4^+$ T cells by following the Fluo4 AM (F14201) and Fura Red (F3020, Invitrogen). A total of 2 μM Fluo4 or 5 μM Fura Red was added to naïve $CD4^+$ T cells, and the cells were incubated at 37 °C for 25 min, followed by washing with DPBS. The calcium flux of anti-CD3 and anti-CD28-coated cells was analyzed in calcium-free HBSS medium (Welgene) by flow cytometry with a measurement time of 300 s (basal time: 0–30 s; activation time (treatment with anti-Armenian hamster IgG secondary antibodies): 50–300 s). Calcium flux measurement using Fura Red was calculated as ratiometric calcium flux (Qdot 655-A/PerCP-Cy5-5-A), with reference to Wendt ER. et al. [38].

Statistical analysis

Data analysis was performed using GraphPad Prism Software 9.0. All data were first analyzed for normality using the Shapiro-Wilk test. Statistical analyses were conducted using various methods, including unpaired two-tailed Student's *t*-test, one sample *t*-test, one-sample Wilcoxon signed rank test, Mann-Whitney test, and one-way or two-way ANOVA. Means are presented as mean ± SD, with p values considered significant as follows: ns, non- significant; $^{*}p<0.05$; $^{**}p<0.01$; $^{***}p<0.001$; and $^{****}p<0.0001$.

Results

IPMK deletion in $CD4^+$ helper T cells attenuates concanavalin A-induced acute hepatitis

To investigate the physiological role of IPMK in the regulation of TCR signaling, we established a mouse model with conditional deletion of IPMK in $CD4^+$ Th cells by crossing *Ipmk* floxed mice ($IPMK^{f/f}$) and CD4-Cre mice ($IPMK^{\Delta CD4}$). The development of T cells in the thymus, lymph node, and spleen is normal in $IPMK^{\Delta CD4}$ mice [34]. Injecting concanavalin A (ConA), a lectin that acts as a TCR agonist [39], is a mouse model widely used to study T cell-dependent hepatitis since it mimics the pathogenesis and pathological symptoms of human autoimmune hepatitis [40, 41]. To examine the biological effects of IPMK on $CD4^+$ T cells in vivo, we applied the ConA-induced hepatitis model to the $IPMK^{f/f}$ and $IPMK^{\Delta CD4}$ mice (Fig. 1A). Levels of the alanine aminotransferase (ALT) and aspartate aminotransferase (AST), indicators of hepatic injury, were found to be lower in $IPMK^{\Delta CD4}$ mice compared to $IPMK^{f/f}$ mice (fig. S1, A and B; Fig. 1, B and C). A reduction in hepatic damage was also observed in the liver and by H&E staining in the $IPMK^{\Delta CD4}$ mice (Fig. 1D). Apoptosis of hepatocytes was also found to be diminished in the $IPMK^{\Delta CD4}$ mice, as determined by the TUNEL assay (Fig. 1E). These results indicated that ConA-induced liver injuries were alleviated in the $IPMK^{\Delta CD4}$ mice.

As hepatitis is induced by the activation of lymphocytes around the liver tissue, we isolated hepatic mononuclear cells (MNCs) and analyzed the levels of relevant cytokines. Although IFNγ remained unchanged, TNFα was shown to decrease in the $IPMK^{\Delta CD4}$ MNCs (fig. S1C and Fig. 1F). Moreover, as ConA-induced acute hepatitis mainly occurs through $CD4^+$ Th cell-dependent experimental hepatic damage [42–44], we measured the changes in cytokine levels in $CD4^+$ Th cells. No

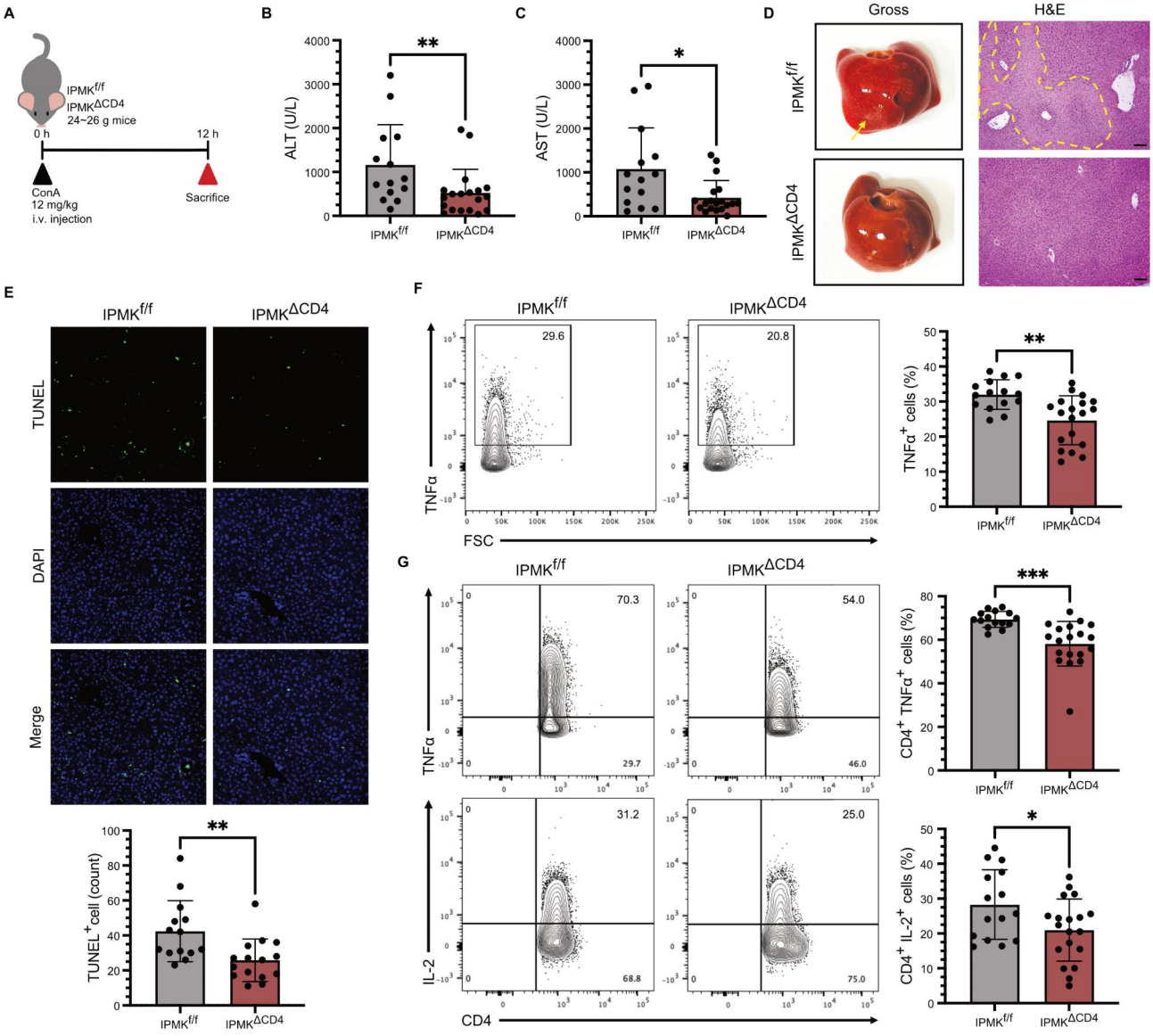

Fig. 1 IPMK deletion in $CD4^+$ helper T cells attenuates Concanavalin A-induced acute hepatitis. (**A**) Schematic diagram of the experimental protocol. A total of 12 mg/kg ConA was injected into the tail vein of 24–26 g mice for 12 h before each mouse was sacrificed ($n \geq 15$ per group). (**B**) Blood ALT levels of sacrificed mice; blood sample was acquired from the retro-orbital vein. (**C**) Blood AST levels of sacrificed mice; blood sample was acquired from the retro-orbital vein. (**D**) The gross mouse liver size and H&E staining of the indicated site are denoted by a yellow arrow. Damaged liver tissue is denoted by a yellow boundary. Scale bar: 100 μm. (**E**) TUNEL stain of ConA-injected mouse liver tissues. (**F**) Flow cytometry analysis of TNFα produced in the liver MNCs of $IPMK^{f/f}$ and $IPMK^{\Delta CD4}$ ConA-injected mice. (**G**) Flow cytometry analysis of TNFα and IL-2 levels in $CD4^+$ cells produced in the liver MNCs of $IPMK^{f/f}$ and $IPMK^{\Delta CD4}$ ConA-injected mice. All flow cytometric plots and images presented are representative of the experiments. The normality of all data was analyzed using the Shapiro-Wilk test. Data are presented as mean ± SD. $^*p < 0.05$; $^{**}p < 0.01$; $^{***}p < 0.001$, using the Mann-Whitney test (**B** and **C**) or unpaired two-tailed Student's *t*-test (**E**, **F**, and **G**) compared to $IPMK^{f/f}$

significant changes were observed in the total $CD4^+$ Th cells (fig. S1D), $CD4^+$ $IFN\gamma^+$ cells, and $CD4^+$ $IL\text{-}4^+$ cells from MNCs between the $IPMK^{f/f}$ and $IPMK^{\Delta CD4}$ mice (fig. S1, E and F). The numbers of both conventional $CD4^+$ Th cells and natural killer T (NKT) cells remained similar between $IPMK^{f/f}$ and $IPMK^{\Delta CD4}$ MNCs (fig. S2A). However, the percentages of $CD4^+$ $TNF\alpha^+$, $CD4^+$ $IL\text{-}2^+$, and $CD4^+$ IL-17 A^+ cells were decreased in $IPMK^{\Delta CD4}$ MNCs (Fig. 1G, fig. S1G, and fig. S2B). These results suggest that IPMK depletion in $CD4^+$ T cells impairs the activation of Th cells and the inflammatory responses associated with ConA stimulation.

IPMK depletion reduces TCR signaling through diminished activation of PLCγ1

Since ConA directly crosslinks with TCR to mimic TCR activation [45], we next measured the TCR signaling response. As PLCγ1 is a major enzyme required for

TCR signaling, we next determined the activation of PLCγ1 and identified the time-dependent phosphorylation of Y783 in PLCγ1 in naïve CD4$^+$ T cells. PLCγ1 Y783 phosphorylation was also found to be impaired in IPMK$^{\Delta CD4}$ naïve CD4$^+$ T cells following direct treatment of ConA (fig. S3A). Directly stimulation using anti-CD3 and anti-CD28 antibodies, a comparison of the ratio of PLCγ1 Y783 phosphorylation at 0 min in each group illustrated that it was reduced in the IPMK$^{\Delta CD4}$ naïve CD4$^+$ T cells (Fig. 2A). Given that calcium is released from intracellular stores as a consequence of PLCγ1 activation, we investigated the influence of IPMK on calcium flux during TCR engagement. Using flow cytometry, we observed diminished activation of IPMK$^{\Delta CD4}$ naïve CD4$^+$ T cells, specifically from the basal state to activation. (Fig. 2B). In addition, we analyzed PKCθ signaling, which is activated by PLCγ1 via its product, DAG. It was found that PKCθ T538 phosphorylation is markedly reduced in TCR-stimulated IPMK$^{\Delta CD4}$ naïve CD4$^+$ T cells (Fig. 2C). A rise in cytosolic calcium and the activation of PKCθ stimulated several transcription factors, including NFAT and NFκB, thereby inducing the expression of cytokines associated with T cell proliferation, such as IL-2. Next, we measured the kinetics of the *Il2* RNA expression level

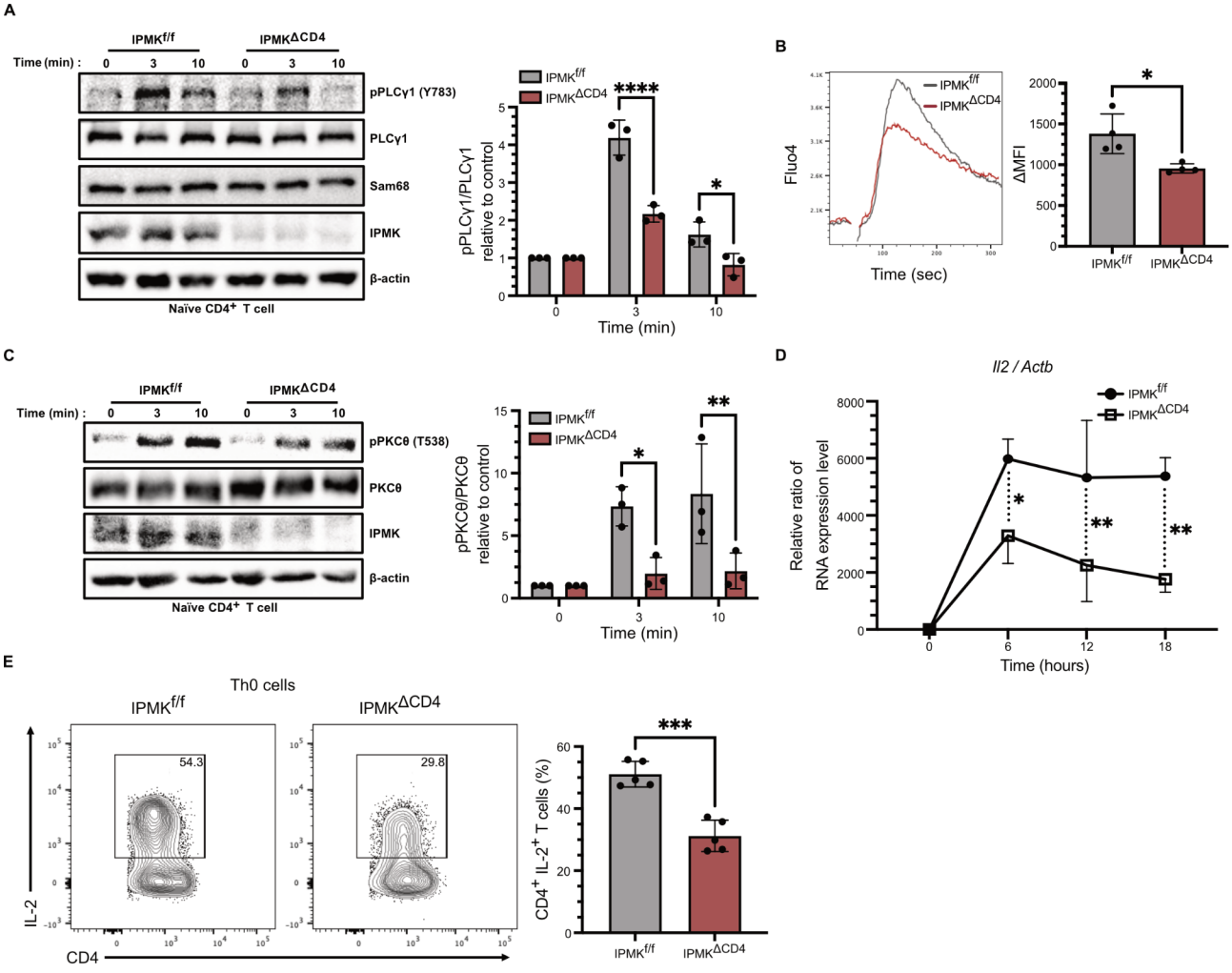

Fig. 2 IPMK depletion reduces TCR signaling through diminished activation of PLCγ1. (**A**) Immunoblot analysis of PLCγ1 and its phosphorylation (Y783) in lysates of naïve CD4$^+$ T cells stimulated with anti-CD3 and anti-CD28 antibodies for 3–10 min. (**B**) Calcium flux of naïve CD4$^+$ T cells activated by anti-CD3, anti-CD28, and anti-Armenian hamster IgG secondary antibodies in calcium-free HBSS. Basal time: 0–30 s; activation time: 50–300 s. ΔMFI was measured as MFI$^{\text{Activation time}}$ – MFI$^{\text{Basal time}}$. (**C**) Immunoblot analysis of PKCθ and its phosphorylation (T538) in lysates of naïve CD4$^+$ T cells stimulated with anti-CD3, anti-CD28, and anti-Armenian hamster IgG secondary antibodies for 3–10 min. (**D**) Quantitative real-time PCR analysis of the expression of *Il2* mRNA in naïve CD4$^+$ T cells polarized into Th0 cells by anti-IFNγ and anti-IL-4 antibodies. (**E**) Flow cytometry analysis of IL-2 in naïve CD4$^+$ T cells polarized into Th0 cells for 16 h by anti-IFNγ and anti-IL-4 antibodies. All blots, kinetics, and flow cytometric plots presented are representative of at least three independent experiments. Densitometric quantitation results were normalized to control conditions. The normality of all data was analyzed using the Shapiro-Wilk test. Data are presented as mean ± SD. $^*p < 0.05$; $^{**}p < 0.01$; $^{***}p < 0.001$; $^{****}p < 0.0001$, using the unpaired two-tailed Student's *t*-test (**B** and **E**) compared to IPMK$^{f/f}$ or two-way ANOVA with Šídák's multiple comparisons test (**A**, **C**, and **D**)

in naïve $CD4^+$ T cells in response to TCR stimulation. Compared to $IPMK^{f/f}$ Th0 cells, $IPMK^{\Delta CD4}$ cells failed to show a robust enhancement in *Il2* RNA expression after 6 h of CD3-CD28 stimulation (Fig. 2D). Consistently, the protein level of IL-2 was decreased in TCR-stimulated $IPMK^{\Delta CD4}$ cells compared to $IPMK^{f/f}$ cells (Fig. 2E). To further investigate the role of IPMK in T cell proliferation, CD3-CD28-activated $IPMK^{f/f}$ and $IPMK^{\Delta CD4}$ Th0 cells were labelled with carboxyfluorescein succinimidyl ester (CFSE). A decrease in CFSE staining intensity was observed in $IPMK^{\Delta CD4}$ $CD4^+$ T cells compared to controls (fig. S3B). Additionally, the level of CD25 was reduced in $IPMK^{\Delta CD4}$ $CD4^+$ T cells, while the level of CD69 remained unchanged (fig. S3, C and D). Overall, these results suggest that IPMK is required for the transmission of TCR-induced $CD4^+$ Th cell signaling and gene expression through PLCγ1 activation.

IPMK regulates PLCγ1 Y783 phosphorylation

We next focused on PLCγ1, as PLC acts as an upstream enzyme of IPMK in InsP metabolism. To dissect the role of IPMK in PLCγ1 activation, we first analyzed PLCγ1 Y783 phosphorylation in mouse embryonic fibroblasts (MEFs). A marked reduction in PLCγ1 Y783 phosphorylation was observed in IPMK KO MEFs (Fig. 3A). A similar reduction in PLCγ1 Y783 phosphorylation was also observed in IPMK KO in NIH3T3 fibroblasts generated via CRISPR/Cas9 editing (Fig. 3B). IPMK KO NIH3T3 fibroblasts also showed reduced PLCγ1 Y783 phosphorylation under the PDGF stimulation condition. However, Y783 phosphorylation was restored by overexpressing wild-type (WT) IPMK in IPMK KO cells (Fig. 3C). Conversely, overexpression of IPMK in HEK293T cells was found to increase PLCγ1 Y783 phosphorylation (Fig. 3D). Collectively, these results further demonstrate the crucial role of IPMK in the regulation of PLCγ1 Y783 phosphorylation.

IPMK is a Sam68-interacting protein

Next, we investigated the molecular mechanism of how IPMK promotes PLCγ1 tyrosine phosphorylation. IPMK performs a pleiotropic role in regulating various signaling pathways, although only a few direct interaction partners are known to serve as IPMK-mediated upstream or downstream mediators. To identify additional IPMK-binding proteins, we previously performed a yeast two-hybrid screening using IPMK as the bait and a human brain cDNA library as the prey [10]. A clone encoding a fusion protein containing the 188–443 region of Sam68 was found to interact with IPMK in the yeast two-hybrid system (Fig. 4, A and B).

Since Sam68 is known as a signaling adaptor that binds to multiple proteins, including PLCγ1 [32, 46], we sought to further characterize this attribute. The physical interaction between IPMK and Sam68 was validated by performing an in vitro binding assay using recombinant proteins. It was observed that purified Sam68 indeed bound to purified human IPMK, confirming a direct protein-protein interaction (Fig. 4C). Additionally, IPMK pull-down experiments were performed using HEK293T cells overexpressing IPMK and Sam68 to confirm this interaction (Fig. 4D). Furthermore, endogenous IPMK and Sam68 proteins were co-immunoprecipitated in MEF lysates, confirming the interaction in vivo (Fig. 4E). To identify the IPMK domains responsible for Sam68 binding, we used a series of IPMK-deleted mutants for co-immunoprecipitation experiments and found that Sam68 interacts with the amino acid regions of 93–182 and 210–426 in IPMK (Fig. 4, F and G), which encompass the inositol phosphate binding site and the kinase domain. To further map the reciprocal binding sites required for IPMK–Sam68 binding, various Sam68-deleted constructs were designed and overexpressed in HEK293T cells (Fig. 4H). In line with the findings from the yeast two-hybrid assay, it was observed that IPMK selectively interacts with the C-terminus of Sam68, with no binding affinity for its N-terminus (Fig. 4I). We further generated Sam68 mutants with deleted tyrosine-rich region (YY) and nucleus localization signal (NLS) domain. IPMK failed to associate with the YY domain-deleted Sam68 mutant (ΔYY) (Fig. 4J), indicating that the YY region of Sam68 is the primary binding site for IPMK.

IPMK stabilizes the interaction between Sam68 and PLCγ1

Direct interaction between IPMK and Sam68 made us speculate whether IPMK is critical for the regulation of Sam68-mediated signaling actions. We first checked the protein level of Sam68 in IPMK KO cells and found no apparent defect (Fig. 3). We next examined whether IPMK is required for stabilizing the formation of the Sam68–PLCγ1 complex. First, we overexpressed IPMK in HEK293T cells and detected both Sam68 and PLCγ1 in the IPMK precipitates along with an increased level of phosphorylated PLCγ1 (Fig. 5A). To analyze the status of the Sam68–PLCγ1 complexes in the presence or absence of IPMK, we next isolated the Sam68 immunoprecipitates from WT ($IPMK^{f/f}$) and IPMK KO MEF lysates. Depletion of IPMK markedly reduced Sam68–PLCγ1 binding without influencing either the Sam68 or PLCγ1 levels (fig. S4A). We also examined the level of Src and found a significantly reduced association among PLCγ1, Sam68, and Src in the PLCγ1 immunoprecipitates from IPMK KO MEFs (Fig. 5B). Furthermore, a decrease in both the Sam68–PLCγ1 interaction and PLCγ1 Y783 phosphorylation was observed in IPMK-depleted NIH3T3 fibroblasts (fig. S4B). Thus, IPMK was found to stabilize the association between Sam68 and PLCγ1, presumably by mediating the recruitment of upstream SFKs, such as Src

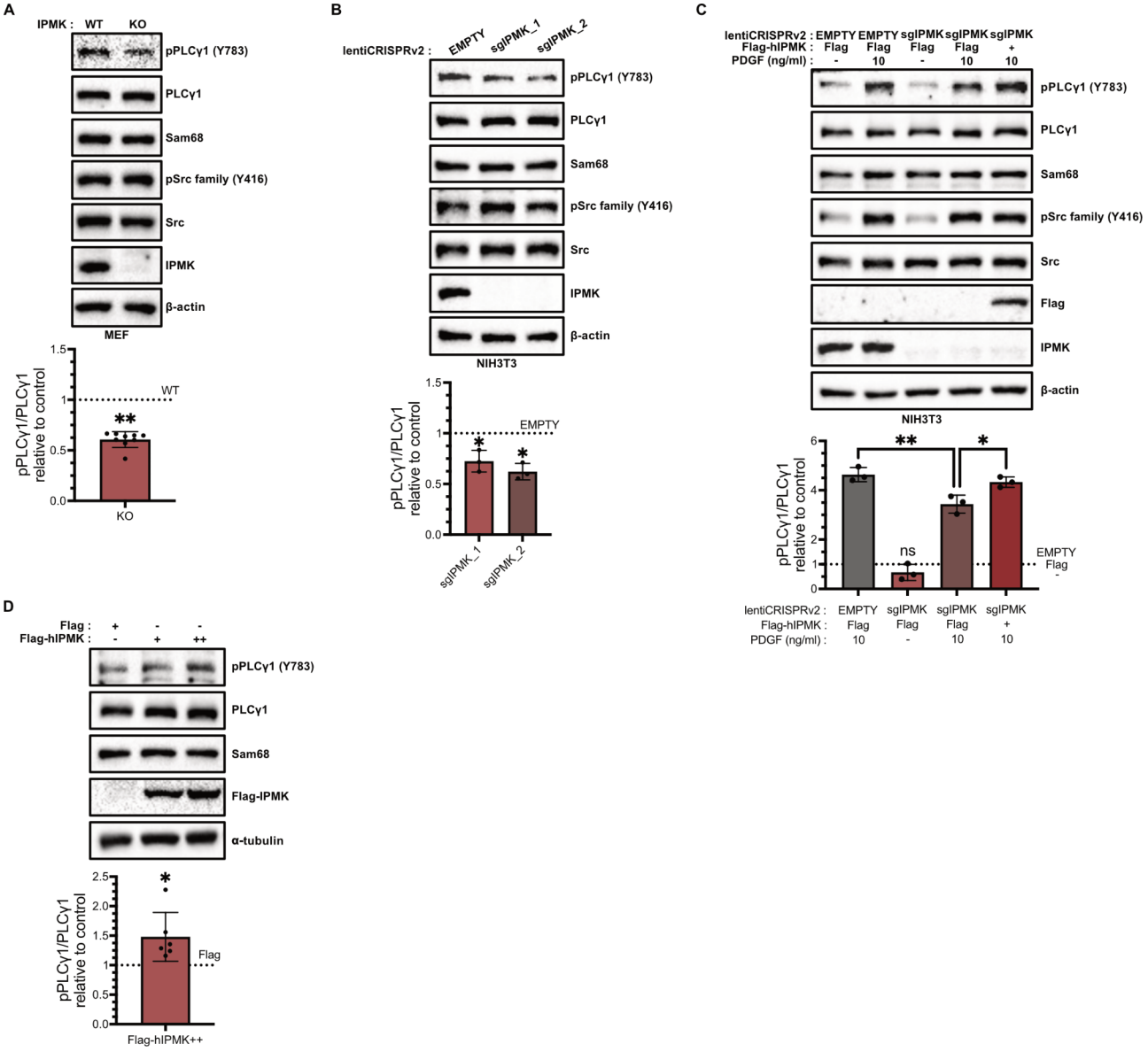

Fig. 3 IPMK regulates PLCγ1 Y783 phosphorylation. (**A**) Immunoblot analysis of PLCγ1 and Src as well as their phosphorylation (Y783 of PLCγ1 and Y416 of Src) in lysates from IPMK KO MEFs. (**B**) Immunoblot analysis of PLCγ1 and Src as well as their phosphorylation (Y783 of PLCγ1 and Y416 of Src) in lysates from CRISPR/Cas9 mediated IPMK KO NIH3T3 cells. (**C**) Immunoblot analysis of PLCγ1 and Src as well as their phosphorylation (Y783 of PLCγ1 and Y416 of Src) in lysates from CRISPR/Cas9-mediated IPMK KO NIH3T3 cells stimulated by PDGF (10 ng/mL) for 10 min after serum starvation for 12 h. ns, non-significant, one-sample *t*-test compared to PDGF-, Flag-transfected NIH3T3 cells. $^{*}p < 0.05$; $^{**}p < 0.01$, one-way ANOVA with Tukey's multiple comparisons test. (**D**) Immunoblot analysis of PLCγ1 and its phosphorylation (Y783) in Flag-hIPMK transfected HEK293T cells at different doses. All blots presented are representative of at least three independent experiments. Densitometric quantitation results were normalized to control conditions. The normality of all data was analyzed using the Shapiro-Wilk test. Data are presented as mean ± SD. ns; $^{*}p < 0.05$; $^{**}p < 0.01$, using the one-sample Wilcoxon signed rank test (**A** and **D**), one-sample *t*-test (**B** and **C**) compared to each control or one-way ANOVA with Tukey's multiple comparisons test (**C**)

to PLCγ1. Furthermore, when NIH3T3 fibroblasts were stimulated by platelet-derived growth factor (PDGF), the amount of IPMK increased in the Sam68 immunoprecipitates (Fig. 5C), suggesting that the formation of the IPMK-Sam68–PLCγ1 complex is induced in response to cellular activation.

To validate the functional significance of Sam68 in PLCγ1 signaling of T cells, we first depleted Sam68 in Jurkat T cells via CRISPR/Cas9 editing. A marked reduction in PLCγ1 phosphorylation was observed in these cells (fig. S4C). To analyze the status of the Sam68–PLCγ1 complexes in CD4^{+} T cells, we isolated the Sam68 immunoprecipitates from the lysates of IPMK$^{f/f}$ and IPMK$^{\Delta CD4}$ naïve CD4^{+} T cells. Depletion of IPMK in CD4^{+} T cells markedly reduced Sam68–PLCγ1 binding without influencing either the Sam68 or PLCγ1

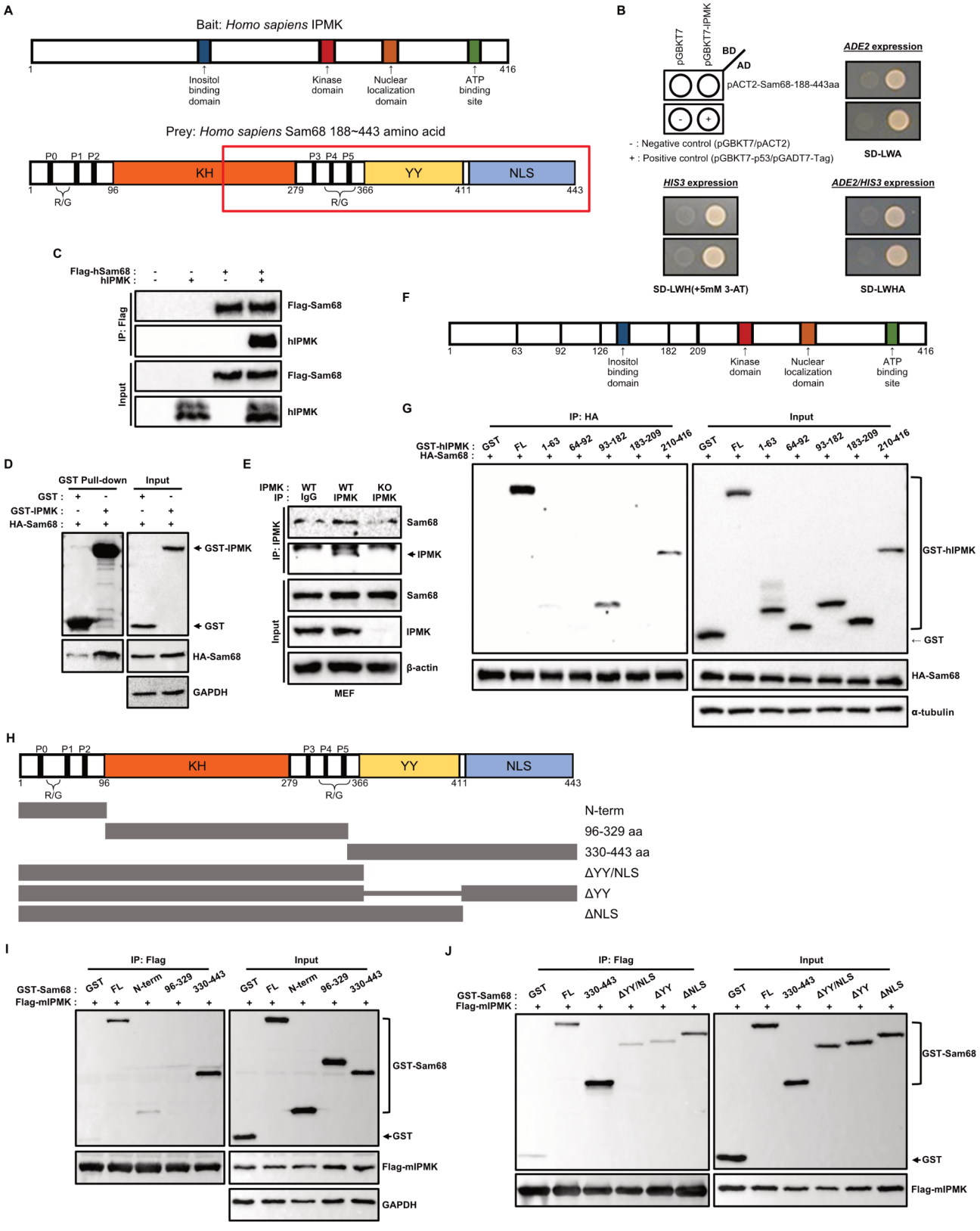

Fig. 4 (See legend on next page.)

(See figure on previous page.)

Fig. 4 IPMK directly interacts with Sam68. (**A**) Schematic diagram of prey and bait for yeast two hybrid screening. The full-length. *Homo sapiens* IPMK was cloned into a pGBKT7 vector to generate a fusion protein that was downstream of the Gal4 DNA binding domain (BD). A pGBKT7 plasmid was used as bait. The 188–443 amino acid of Sam68 (red-frame box) was cloned into the pACT2 vector to form a fusion protein that was downstream of the Gal4 activation domain (AD). A pACT2 plasmid was used as prey. (**B**) The AH109 yeast strain was co-transformed with either pGBKT7 or pGBKT7-IPMK and pACT2-Sam68-188-443aa. Yeast cells were incubated in SD-LW media, with either adenine removed (SD-LWA), histidine removed (SD-LWH), and both removed (SD-LWHA). SD-LWH media had 5 mM 3-amino-1,2,4 triazole(3-AT) added to it. The gene expressions of ADE2 and HIS3 were examined to identify any positive clones. pGBKT7-p53 and pGADT7 plasmids were used as positive controls. (**C**) In vitro binding assay between purified Flag-human Sam68 (hSam68) protein and purified human IPMK (hIPMK) protein. Anti-Flag M2 beads were used for immunoprecipitation. (**D**) GST pull-down assay and immunoblot were used to analyze the interaction between GST-IPMK and HA-Sam68 following their co-transfection in HEK293T cells. (**E**) Endogenous co-IP test and immunoblot on IPMK and Sam68 in MEFs. The cell lysate was immunoprecipitated with anti-IPMK antibodies. (**F**) Schematic depiction of IPMK domains. Numbers either indicate the start or final amino acids in each fragment. (**G**) IPMK mapping analysis of IPMK fragments or full-length (FL) protein interacting with HA-Sam68 following co-transfection in HEK293T cells. Anti-HA antibodies were used for the co-IP test. (**H**) Schematic depiction of Sam68 domains and fragments. Numbers indicate the start or final amino acids for each fragment. KH: hnRNPK homology domain; YY: tyrosine-rich region; NLS: nucleus localization sequence; P1–6: proline-rich region; R/G: arginine/glycine-rich region. (**I** and **J**) Sam68 mapping analysis using Sam68 fragments or full-length (FL) protein, and Flag-mouse IPMK (mIPMK) co-transfected HEK293T cells. Anti-Flag M2 beads were used for the co-IP test. All blots presented are representative of at least three independent experiments

levels (Fig. 5D). However, the level of another signaling adaptor, linker for activation of T cells (LAT), remained unchanged in the PLCγ1 immunoprecipitates from $IPMK^{\Delta CD4}$ naïve $CD4^+$ T cells compared to controls (fig. S4D). Similar to PDGF-stimulation in NIH3T3 cells, T cell stimulation led to an increase in IPMK in the PLCγ1–Sam68 co-immunoprecipitates from T cells (fig. S4E). These results suggest that IPMK is critical for mediating PLCγ1 phosphorylation and activation of naïve $CD4^+$ T cells by stabilizing the Sam68–PLCγ1 interaction.

IPMK non-catalytically promotes PLCγ1 phosphorylation

Next, we investigated the hypothesis that IPMK acts as a scaffold to regulate PLCγ1 phosphorylation via the IPMK-Sam68 interaction. Based on the Sam68–IPMK binding studies shown in Fig. 4, we employed the Sam68-binding IPMK fragment 93–182 as a dominant-negative (DN) mutant. The overexpression of this GST-tagged dominant-negative IPMK peptide (IPMK-DN) in fibroblasts reduced the association of Sam68 with both endogenous IPMK and PLCγ1 (Fig. 6A). Under this condition, the phosphorylation of PLCγ1 Y783 was markedly decreased following the expression of IPMK-DN (Fig. 6B).

Next, we further examined whether this IPMK scaffolding action can be recapitulated by purified proteins in vitro. Using in vitro kinase assays with PLCγ1 as the substrate, treatment with either wild-type or catalytically-inactive mutant IPMK (K129A) proteins markedly increased the Src-catalyzed phosphorylation of Y783 in PLCγ1 (Fig. 6C). Collectively, these results suggest that IPMK non-catalytically mediates PLCγ1 phosphorylation by acting as a scaffold that functionally recruits Sam68-associated SFKs to PLCγ1 (Fig. 6D).

Inhibiting the IPMK-Sam68 protein interaction suppresses PLCγ1 phosphorylation in T cells

To further validate our hypothesis for $CD4^+$ Th cells, we also overexpressed the IPMK-DN peptide via viral transduction to achieve high expression efficiency (Fig. 7A and fig. S5A). The levels of Sam68 and IPMK in the PLCγ1 immunoprecipitates were found to be decreased in CD3/CD28-stimulated IPMK-DN–overexpressing T cells compared to controls (Fig. 7B), indicating impaired formation of the PLCγ1/Sam68/IPMK protein complex. Compared to empty vector-transduced control cells, IPMK-DN–overexpressing T cells showed reductions in PLCγ1 Y783 phosphorylation, calcium flux, and expression of IL-2 and CD25 (Fig. 7, C-E and fig. S5B). We therefore concluded that IPMK-DN interferes with the stability of the protein complex, inhibits PLCγ1 activation, and impairs T cell activation.

We also generated a cell-permeable form of the IPMK-DN peptide. Compared to the IPMK 93–182 fragment, the shorter fragment of IPMK 93–126 was shown to efficiently lower PLCγ1 phosphorylation in fibroblasts (fig. S5C). This peptide was fused to the protein transduction domain (PTD), which promotes cell-permeable peptide delivery [47]. Naïve $CD4^+$ T cells were treated with either control PTD or PTD–IPMK 93–126 (PTD_93–126) peptides and stimulated by anti-CD3 and anti-CD28 antibodies (Fig. 7F). The delivery of the cell-permeable PTD_93–126 fragment significantly decreased PLCγ1 Y783 phosphorylation in naïve $CD4^+$ T cells in response to TCR activation (Fig. 7G). The level of IL-2 was also decreased in $CD4^+$ T cells treated with PTD_93–126 (Fig. 7H). Thus, these results corroborate the notion that the direct association of IPMK with Sam68 mediates SFK-stimulated PLCγ1 phosphorylation, thereby enhancing TCR signaling (Fig. 8).

Discussion

Our study establishes that IPMK is a physiologic determinant of PLCγ1 activation and its downstream signaling. IPMK was identified as a direct binding target of Sam68, which acts as a signaling scaffold that is responsible for linking SFKs with PLCγ1. Mapping studies showed reciprocal interactions between the YY domain of Sam68 and

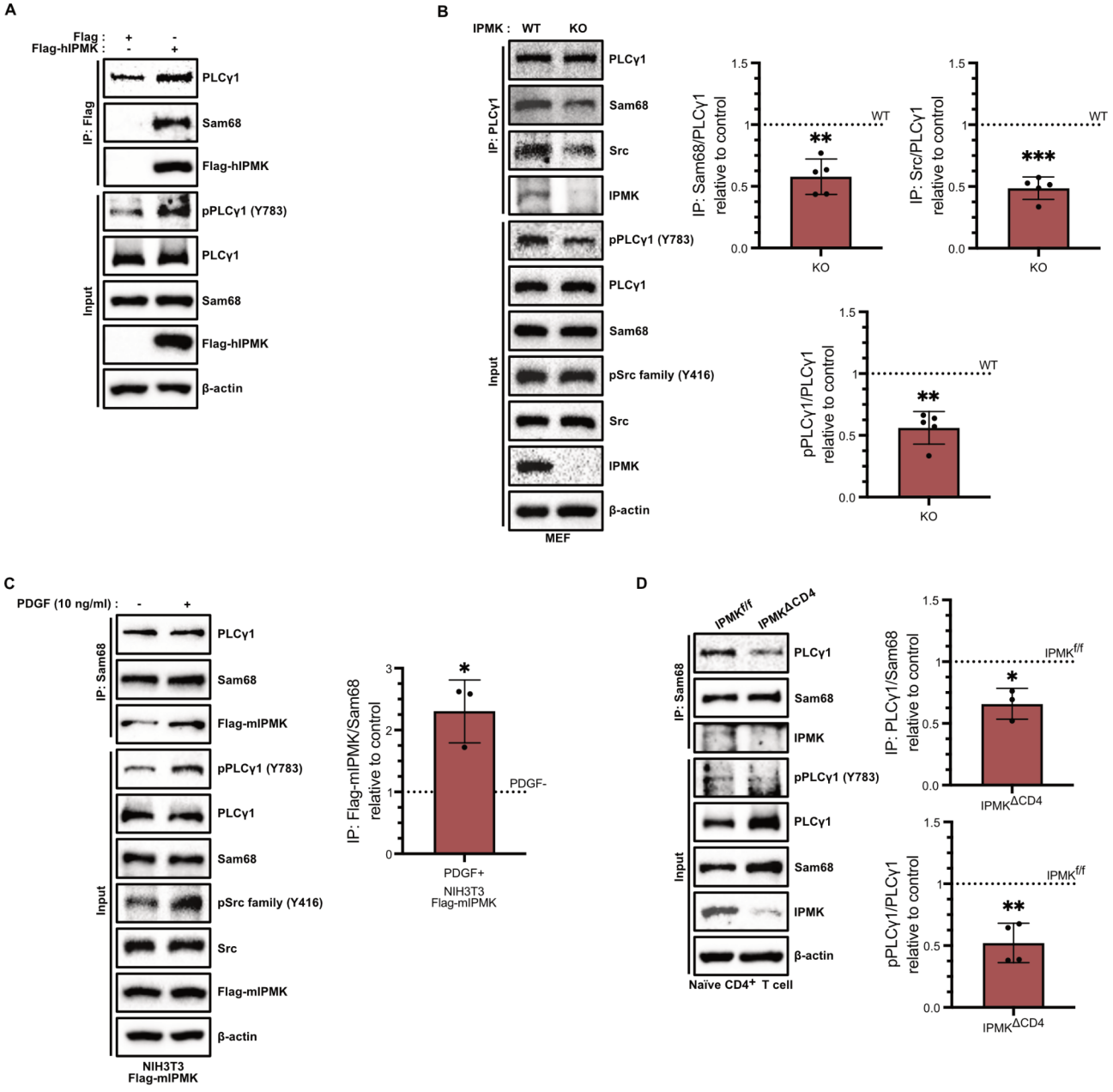

Fig. 5 IPMK stabilizes the interaction between Sam68 and PLCγ1. (**A**) Overexpression co-IP test and immunoblot analysis for PLCγ1, Sam68, and IPMK in Flag-hIPMK transfected HEK293T cells. The cell lysate was immunoprecipitated with anti-Flag M2 beads. (**B**) Endogenous co-IP test and immunoblot analysis for PLCγ1, Sam68, Src, and IPMK in IPMK KO MEFs. The cell lysates were immunoprecipitated with anti-PLCγ1 antibodies. (**C**) Overexpression co-IP test and immunoblot analysis for PLCγ1, Sam68, and IPMK in Flag-mIPMK transfected NIH3T3 cells following PDGF (10 ng/mL) stimulation for 3 min after serum starvation for 12 h. The cell lysate was immunoprecipitated with anti-Sam68 antibodies. (**D**) Endogenous co-IP test and immunoblot analysis for PLCγ1, Sam68, and IPMK in naïve CD4$^+$ T cells. The cell lysate was immunoprecipitated with anti-Sam68 antibodies. All blots presented are representative of at least three independent experiments. Densitometric quantitation results were normalized to control conditions. The normality of all data was analyzed using the Shapiro-Wilk test. Data are presented as mean ± SD. $^{*}p < 0.05$; $^{**}p < 0.01$; $^{***}p < 0.001$, using the one-sample *t*-test compared to each control

the InsP kinase domain of IPMK. The depletion of IPMK in fibroblasts or CD4$^+$ Th cells reduced the phosphorylation of PLCγ1 Y783 following TCR engagement or PDGF stimulation. We elucidated a mechanism underlying IPMK-mediated regulation of PLCγ1 activation. We report that IPMK depletion in CD4$^+$ Th cells destabilizes the interaction between PLCγ1 and the Sam68 scaffold. This reduction in PLCγ1–Sam68 binding downregulates efficient PLCγ1 phosphorylation by Sam68-associated SFKs, such as Fyn and Src, thereby leading to a decrease in both calcium influx and the PLC-dependent downstream signaling responses, such as PKC activation. In

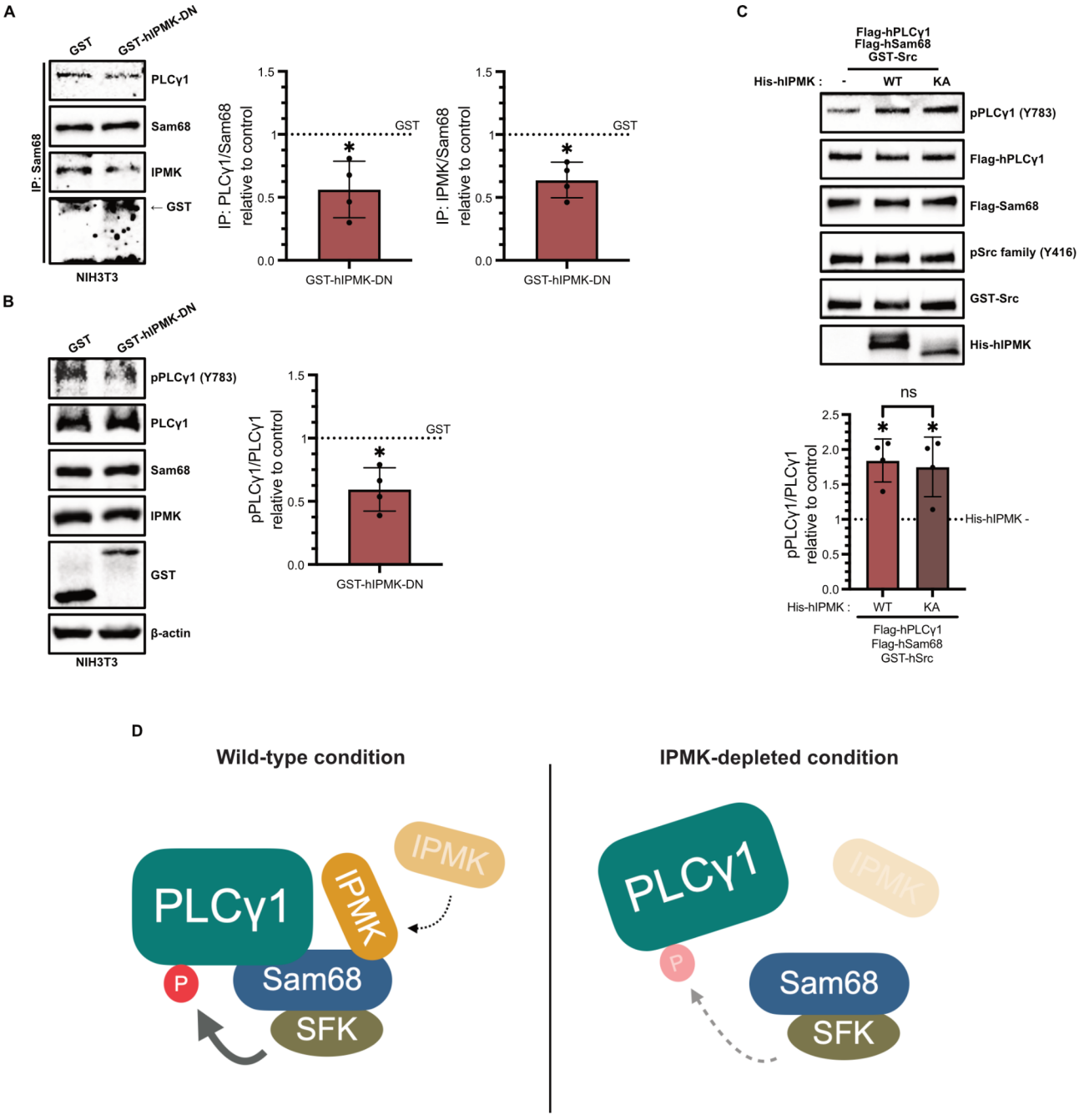

Fig. 6 IPMK non-catalytically promotes PLCγ1 phosphorylation. (**A**) Overexpression co-IP test and immunoblot analysis for PLCγ1, Sam68, and IPMK in GST-hIPMK-DN transfected NIH3T3 cells. The cell lysate was immunoprecipitated with anti-Sam68 antibodies. (**B**) Immunoblot analysis of PLCγ1 and its phosphorylation (Y783) in GST-hIPMK-DN transfected NIH3T3 cell lysates. (**C**) In vitro kinase assay and immunoblot analysis using PLCγ1, Sam68, Src, and IPMK WT/KA recombinant proteins. IPMK and ATP were added following the formation of the PLCγ1–Sam68–Src protein complex. $^{*}p < 0.05$, one-sample *t*-test compared to control; ns, non-significant, unpaired two-tailed Student's *t*-test between His-hIPMK WT and KA. (**D**) Schematic depiction of PLCγ1–Sam68–Src complex formation for PLCγ1 phosphorylation with or without IPMK. All blots presented are representative of at least three independent experiments. Densitometric quantitation results were normalized to control conditions. The normality of all data was analyzed using the Shapiro-Wilk test. Data are presented as mean ± SD. ns; $^{*}p < 0.05$, using the one-sample *t*-test (**A-C**) and unpaired two-tailed Student's *t*-test (**C**) compared to each control

vitro kinase assays indicated that either wild-type or catalytically-inactive mutant IPMK proteins promote Src-mediated PLCγ1 phosphorylation, demonstrating that IPMK performs a direct, non-catalytic action. Overexpression of a Sam68-binding IPMK-DN fragment interfered with the PLCγ1–Sam68 interaction and PLCγ1 phosphorylation, which suggests the functional significance of the IPMK–Sam68 interaction in TCR signaling.

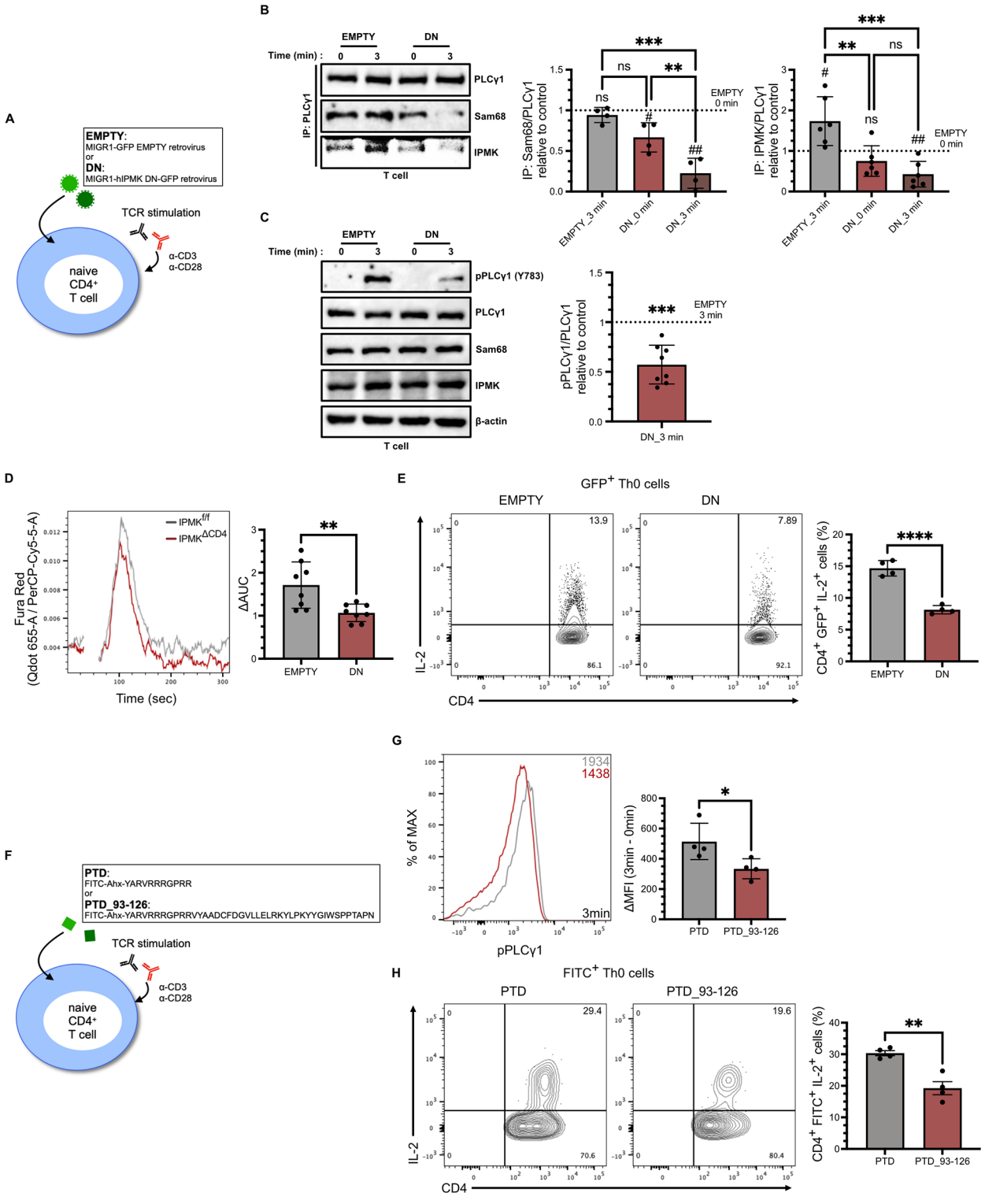

Fig. 7 (See legend on next page.)

(See figure on previous page.)

Fig. 7 Inhibiting IPMK–Sam68 protein interaction suppresses PLCγ1 phosphorylation in T cells. (**A**) Schematic depiction of the transduction strategy for MIGR1-GFP EMPTY or MIGR1-hIPMK DN-GFP retrovirus transduction into naïve $CD4^+$ T cells and TCR stimulation using anti-CD3, anti-CD28, and anti-Armenian hamster IgG secondary antibodies. (**B**) Endogenous co-IP test and immunoblot analysis for PLCγ1, Sam68, and IPMK in hIPMK-DN transduced T cells, under TCR stimulation and non-stimulation conditions. The cell lysates were immunoprecipitated using anti-PLCγ1 antibodies. ns; $^{\#}p < 0.05$; $^{\#\#}p < 0.01$, one-sample *t*-test compared to control: EMPTY viral vector transduced TCR- T cells. ns; $^{**}p < 0.01$; $^{***}p < 0.001$, one-way ANOVA with Tukey's multiple comparisons test. (**C**) Immunoblot analysis of PLCγ1 and its phosphorylation (Y783) in hIPMK-DN transduced T cells, under TCR stimulation and non-stimulation conditions. (**D**) Calcium flux of virus-transduced GFP^+ $CD4^+$ T cells activated by anti-CD3, anti-CD28, and anti-Armenian hamster IgG secondary antibodies in calcium-free HBSS. Basal time: 0–30s; activation time: 60–310s. ΔAUC was measured as $AUC^{\text{Activation time}} - AUC^{\text{Basal time}}$. (**E**) Flow cytometry analysis of IL-2 in virus-transduced GFP^+ $CD4^+$ T cells polarized into Th0 cells using anti-IFNγ and anti-IL-4 antibodies followed by treatment with brefeldin A for four hours. (**F**) Schematic depiction of the transduction strategy for PTD or PTD_93–126 into naïve $CD4^+$ T cells and TCR stimulation using anti-CD3, anti-CD28, and anti-Armenian hamster IgG secondary antibodies. (**G**) Flow cytometry analysis of phospho-PLCγ1 (Y783) in 1 μM PTD or PTD_93–126 transduced naïve $CD4^+$ T cells following TCR stimulation as described (**F**). ΔMFI was measured as (MFI of each 3-minute samples) – (average of 0-minute samples). (**H**) Flow cytometry analysis of IL-2 in PTD peptide-transduced $FITC^+$ $CD4^+$ T cells polarized into Th0 cells using anti-IFNγ and anti-IL-4 antibodies. All blots and flow cytometric plots presented are representative of at least three independent experiments. Densitometric quantitation results were normalized to control conditions. The normality of all data was analyzed using the Shapiro-Wilk test. Data are presented as mean ± SD. ns; $^{*}p < 0.05$; $^{**}p < 0.01$; $^{***}p < 0.001$; $^{****}p < 0.0001$, using the one-sample *t*-test (**B** and **C**), unpaired two-tailed Student's *t*-test (**D-E** and **G-H**) compared to each control or one-way ANOVA with Tukey's multiple comparisons test (**B**)

In a mouse model of hyperactivated TCR-induced autoimmune hepatitis, conditional deletion of IPMK in $CD4^+$ Th cells significantly decreased liver injury and immune responses.

PLCγ1 is recruited by upstream regulators, such as LAT, in response to TCR stimulation, while the phosphorylation of PLCγ1 activates downstream signaling molecules [17]. Sam68 was previously suggested as one of the scaffolds that link the SFKs, such as Src, with PLCγ1 [23, 29, 31]. Based on our model (Fig. 8), upon cellular activation, IPMK binds to Sam68, thereby facilitating the formation of the functional Sam68–PLCγ1 complex. The increased binding of IPMK to Sam68 allows the SFKs to efficiently catalyze the phosphorylation of PLCγ1 and the activation of downstream signaling events. Thus, the loss of IPMK in $CD4^+$ Th cells causes a decrease in PLCγ1 phosphorylation, thereby limiting the full activation of calcium flux and PKC signaling to diminish the production of inflammatory cytokines (e.g., IL-2) and their associated immune responses. Our results propose a signaling role of IPMK in $CD4^+$ Th cells by demonstrating that IPMK acts as a Sam68-binding partner that regulates TCR signaling events by modulating the PLCγ1 activity. Further studies are needed to examine whether this IPMK–Sam68 binding influences other upstream factors, such as Itk.

The receptor-mediated PLCγ1 activation involves its phosphorylation by receptor tyrosine kinase or non-receptor tyrosine kinases, such as SFKs, in response to the activation of various growth factor receptors and immune receptors, including TCR [15, 48, 49]. Despite the fundamental function of PLCγ1 in T cells, the mechanism of PLCγ1 activation following TCR stimulation is incompletely understood. Tyrosine phosphorylation in the CD3 chain by lymphocyte protein tyrosine kinase (Lck) recruits ζ-chain-associated protein kinase of 70 kDa (ZAP70), followed by phosphorylation of the transmembrane adaptor molecule LAT [21]. TCR engagement results in the identification of LAT as the primary docking site for PLCγ1. The binding of PLCγ1 to LAT is specifically mediated by the N-terminal SH2 domain in PLCγ1, which interacts with phosphorylated LAT. Indeed, the proline-rich motif in Sam68 was also identified to interact with the SH3 domain in PLCγ1 [46]. The phosphorylation of tyrosine in Sam68 by SFKs increases the Sam68–PLCγ1 interaction. Our demonstration underscores the crucial role of IPMK in facilitating PLCγ1 phosphorylation in a manner dependent on the binding between Sam68 and IPMK. This highlights the necessity of devoting continuous efforts to precisely elucidate the intricate molecular interactions among IPMK, Sam68, PLCγ1, and other factors already identified. In addition, the results of this study expand our understanding by generalizing the role of IPMK in the activation of PLCγ1 in PDGF-stimulated fibroblasts. Hence, we suggest a regulatory model for PLCγ1 in both T cells and fibroblasts that integrates our recent discoveries along with previously documented results.

The functional interplay between IPMK and Sam68 identified in this study elucidates a previously undisclosed mechanism, demonstrating that IPMK stabilizes the Sam68–PLCγ1 complex. This stabilization, in turn, enhances the TCR signaling responses mediated by PLCγ1. Notably, we demonstrate that this regulatory function operates independently of IPMK's catalytic activity; instead, it relies on dynamic protein–protein interactions between IPMK and Sam68. Therefore, in addition to its catalytic involvement in inositol phosphate metabolism and its scaffolding role in various signaling pathways, IPMK serves as a pivotal regulatory checkpoint for PLCγ1-dependent immunoregulation. Given the recent identification of single-nucleotide polymorphisms (SNPs) in IPMK associated with immune diseases, such as rheumatoid arthritis, psoriasis, and Crohn's disease [50, 51], we aim to focus their potential impact. We anticipate that interventions that modulate the IPMK level or

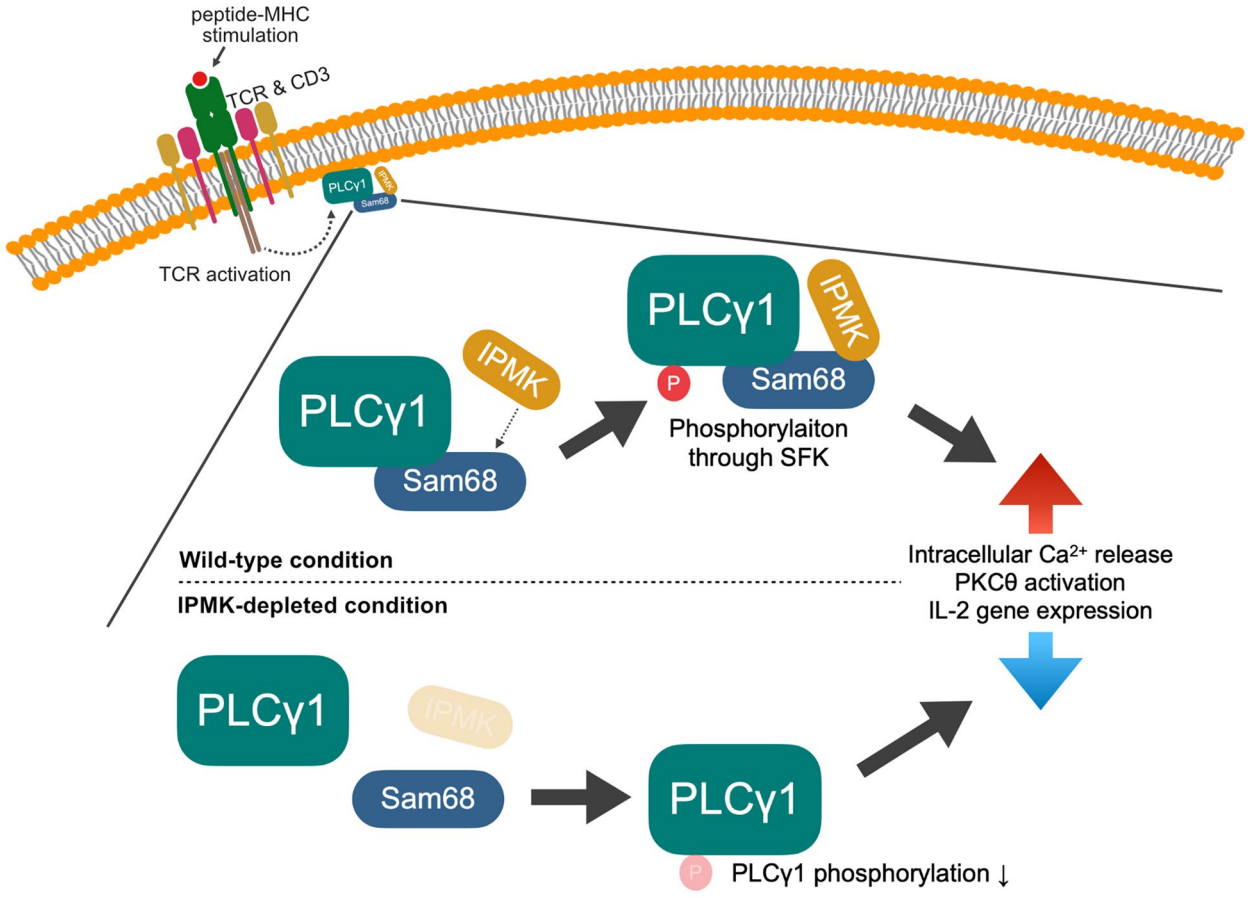

Fig. 8 Graphical summary demonstrating the stabilization of the PLCγ1–Sam68 protein complex by IPMK in TCR-stimulated $CD4^+$ Th cells

IPMK's interaction with Sam68 may be beneficial in the treatment and control of unregulated immune diseases.

Conclusion

Our study highlights the pivotal role of IPMK in regulating PLCγ1 activation triggered by TCR signaling in T cells. Depletion of IPMK in $CD4^+$ helper T cells mitigated ConA-induced hepatic injury in mice. Mechanistic investigations unveiled that IPMK promotes PLCγ1 activation by enhancing the stability of the Sam68–PLCγ1 complex. Consequently, our findings offer novel insights into the molecular mechanisms governing PLCγ1 activation. Targeting IPMK specifically emerges as a promising therapeutic strategy for diseases associated with hyperactive TCR signaling.

Abbreviations

ALT	Alanine aminotransferase
AMPK	Adenosine 5′-monophosphate–activated protein kinase
AST	Aspartate aminotransferase
Btk	Bruton's tyrosine kinase
ConA	Concanavalin A
DAG	Diacylglycerol
DN	Dominant-negative
$InsP_3$	Inositol 1,4,5-trisphosphate
IPMK	Inositol polyphosphate multikinase
Itk	Interleukin-2-inducible T-cell kinase
KHDRBS1	KH domain containing RNA binding signal transduction associated 1 (another name of Sam68)
MEFs	Mouse embryonic fibroblasts
MNCs	Mononuclear cells
mTOR	Mechanistic target of rapamycin
NFAT	Nuclear factor of activated T cells
PDGF	Platelet-derived growth factor
PIP_2	Phosphatidylinositol 4,5-bisphosphate
PIP_3	Phosphatidylinositol 3,4,5-trisphosphate
PKCθ	Protein kinase C theta
PLCγ1	Phospholipase C gamma 1
PTD	Protein transduction domain
Sam68	Src-associated substrate during mitosis of 68 kDa
SFKs	Src family kinases
SRF	Serum response factor
STAR family	Signal transduction and activation of the RNA family
TCR	T cell receptor
TRAF6	Tumor necrosis factor receptor–associated factor 6
TUNEL assay	Terminal deoxynucleotidyl transferase dUTP nick end labeling assay

Supplementary Information

The online version contains supplementary material available at https://doi.org/10.1186/s12964-024-01907-0.

Supplementary Material 1

Acknowledgements
We thank all the members of the Kim lab for discussion.

Author contributions
S.H. and S.K. designed the experiments and analyzed the results. S.H., K.K., Y-R.S., J.P., and S.E.C. carried out the experiments. H.M., S.L., J-J.S., S-J.K., W-I.J., R.H.S. provided reagents and comments. S.H. and S.K. wrote the manuscript. S.K. supervised the research.

Funding
This work was supported by the National Research Foundation of Korea (NRF-2018R1A5A1024261, NRF-2020R1A2C3005765, and RS-2023-00278918, RS-2024-00415888 to S.K.) and the KAIST Key Research Institutes Project (Interdisciplinary Research Group).

Data availability
All data needed to evaluate the conclusions in the paper are present in the paper and/or the Supplementary Materials. Additional data related to this paper may be requested from the authors.

Declarations

Ethics approval and consent to participate
The animal protocols conducted adhered to approved guidelines established by the KAIST Animal Care and Use Committee (KAIST, KA2018-52).

Consent for publication
Not applicable.

Competing interests
The authors declare no competing interests.

Author details
[1]Department of Biological Sciences, Korea Advanced Institute of Science and Technology (KAIST), Youseong-Gu, Daejeon 34141, Republic of Korea
[2]Graduate School of Medical Science and Engineering, Korea Advanced Institute of Science and Technology (KAIST), Youseong-Gu, Daejeon 34141, Republic of Korea
[3]School of Biological Sciences, Institute of Molecular Biology and Genetics, Seoul National University, Seoul 08826, Republic of Korea
[4]KAIST Institute for the BioCentury, KAIST, Daejeon 34141, Republic of Korea
[5]KAIST Stem Cell Center, KAIST, Daejeon 34141, Republic of Korea

Received: 26 April 2024 / Accepted: 22 October 2024
Published online: 30 October 2024

References

1. Kim S, Bhandari R, Brearley CA, Saiardi A. The inositol phosphate signalling network in physiology and disease. Trends Biochem Sci. 2024.
2. Saiardi A, Erdjument-Bromage H, Snowman AM, Tempst P, Snyder SH. Synthesis of diphosphoinositol pentakisphosphate by a newly identified family of higher inositol polyphosphate kinases. Curr Biol. 1999;9(22):1323–6.
3. Kim E, Beon J, Lee S, Park SJ, Ahn H, Kim MG, et al. Inositol polyphosphate multikinase promotes Toll-like receptor-induced inflammation by stabilizing TRAF6. Sci Adv. 2017;3(4):e1602296.
4. Lee H, Kim E, Kim S. miRNA-Induced Downregulation of IPMK in Macrophages Mediates Lipopolysaccharide-Triggered TLR4 Signaling. Biomolecules. 2023;13(2).
5. Kim W, Kim E, Min H, Kim MG, Eisenbeis VB, Dutta AK, et al. Inositol polyphosphates promote T cell-independent humoral immunity via the regulation of Bruton's tyrosine kinase. Proc Natl Acad Sci U S A. 2019;116(26):12952–7.
6. Min H, Kim W, Hong S, Lee S, Jeong J, Kim S, et al. Differentiation and homeostasis of effector Treg cells are regulated by inositol polyphosphates modulating Ca(2+) influx. Proc Natl Acad Sci U S A. 2022;119(27):e2121520119.
7. Kim S, Kim SF, Maag D, Maxwell MJ, Resnick AC, Juluri KR, et al. Amino Acid Signaling to mTOR Mediated by Inositol Polyphosphate Multikinase. Cell Metabol. 2011;13(2):215–21.
8. Bang S, Kim S, Dailey MJ, Chen Y, Moran TH, Snyder SH, et al. AMP-activated protein kinase is physiologically regulated by inositol polyphosphate multikinase. Proc Natl Acad Sci U S A. 2012;109(2):616–20.
9. Xu R, Sen N, Paul BD, Snowman AM, Rao F, Vandiver MS, et al. Inositol polyphosphate multikinase is a coactivator of p53-mediated transcription and cell death. Sci Signal. 2013;6(269):ra22.
10. Beon J, Han S, Yang H, Park SE, Hyun K, Lee SY et al. Inositol polyphosphate multikinase physically binds to the SWI/SNF complex and modulates BRG1 occupancy in mouse embryonic stem cells. eLife. 2022;11.
11. Kim E, Tyagi R, Lee JY, Park J, Kim YR, Beon J, et al. Inositol polyphosphate multikinase is a coactivator for serum response factor-dependent induction of immediate early genes. Proc Natl Acad Sci U S A. 2013;110(49):19938–43.
12. Rhee SG. Regulation of phosphoinositide-specific phospholipase C. Annu Rev Biochem. 2001;70:281–312.
13. Brownlie RJ, Zamoyska R. T cell receptor signalling networks: branched, diversified and bounded. Nat Rev Immunol. 2013;13(4):257–69.
14. Poulin B, Sekiya F, Rhee SG. Intramolecular interaction between phosphorylated tyrosine-783 and the C-terminal Src homology 2 domain activates phospholipase C-gamma1. Proc Natl Acad Sci U S A. 2005;102(12):4276–81.
15. Kim HK, Kim JW, Zilberstein A, Margolis B, Kim JG, Schlessinger J, et al. PDGF stimulation of inositol phospholipid hydrolysis requires PLC-gamma 1 phosphorylation on tyrosine residues 783 and 1254. Cell. 1991;65(3):435–41.
16. Noh DY, Shin SH, Rhee SG. Phosphoinositide-specific phospholipase C and mitogenic signaling. Biochim Biophys Acta. 1995;1242(2):99–113.
17. Courtney AH, Lo WL, Weiss A. TCR Signaling: Mechanisms of Initiation and Propagation. Trends Biochem Sci. 2018;43(2):108–23.
18. Gaud G, Lesourne R, Love PE. Regulatory mechanisms in T cell receptor signalling. Nat Rev Immunol. 2018;18(8):485–97.
19. Fu G, Chen Y, Yu M, Podd A, Schuman J, He Y, et al. Phospholipase C{gamma}1 is essential for T cell development, activation, and tolerance. J Exp Med. 2010;207(2):309–18.
20. Navarro MN, Cantrell DA. Serine-threonine kinases in TCR signaling. Nat Immunol. 2014;15(9):808–14.
21. Wang H, Kadlecek TA, Au-Yeung BB, Goodfellow HE, Hsu LY, Freedman TS, et al. ZAP-70: an essential kinase in T-cell signaling. Cold Spring Harb Perspect Biol. 2010;2(5):a002279.
22. Kadamur G, Ross EM. Mammalian phospholipase C. Annu Rev Physiol. 2013;75:127–54.
23. Paronetto MP, Venables JP, Elliott DJ, Geremia R, Rossi P, Sette C. Tr-kit promotes the formation of a multimolecular complex composed by Fyn, PLCgamma1 and Sam68. Oncogene. 2003;22(54):8707–15.
24. Cocco L, Follo MY, Manzoli L, Suh PG. Phosphoinositide-specific phospholipase C in health and disease. J Lipid Res. 2015;56(10):1853–60.
25. Bielli P, Busà R, Paronetto MP, Sette C. The RNA-binding protein Sam68 is a multifunctional player in human cancer. Endocrine-related Cancer. 2011;18(4):R91–102.
26. Najib S, Martin-Romero C, Gonzalez-Yanes C, Sanchez-Margalet V. Role of Sam68 as an adaptor protein in signal transduction. Cell Mol Life Sci. 2005;62(1):36–43.
27. Vogel G, Richard S. Emerging roles for Sam68 in adipogenesis and neuronal development. RNA Biol. 2012;9(9):1129–33.
28. Huot ME, Vogel G, Zabarauskas A, Ngo CT, Coulombe-Huntington J, Majewski J, et al. The Sam68 STAR RNA-binding protein regulates mTOR alternative splicing during adipogenesis. Mol Cell. 2012;46(2):187–99.
29. Fusaki N, Iwamatsu A, Iwashima M, Fujisawa J. Interaction between Sam68 and Src family tyrosine kinases, Fyn and Lck, in T cell receptor signaling. J Biol Chem. 1997;272(10):6214–9.
30. Lang V, Mège D, Semichon M, Gary-Gouy H, Bismuth G. A dual participation of ZAP-70 and scr protein tyrosine kinases is required for TCR-induced tyrosine phosphorylation of Sam68 in Jurkat T cells. Eur J Immunol. 1997;27(12):3360–7.
31. Shen Z, Batzer A, Koehler JA, Polakis P, Schlessinger J, Lydon NB, et al. Evidence for SH3 domain directed binding and phosphorylation of Sam68 by Src. Oncogene. 1999;18(33):4647–53.
32. Jabado N, Jauliac S, Pallier A, Bernard F, Fischer A, Hivroz C. Sam68 association with p120GAP in CD4 + T cells is dependent on CD4 molecule expression. J Immunol. 1998;161(6):2798–803.
33. Feuillet V, Semichon M, Restouin A, Harriague J, Janzen J, Magee A, et al. The distinct capacity of Fyn and Lck to phosphorylate Sam68 in T cells is essentially governed by SH3/SH2-catalytic domain linker interactions. Oncogene. 2002;21(47):7205–13.

34. Yuk CM, Kim D, Hong S, Kim M, Jeong H-W, Park SJ et al. Inositol polyphosphate multikinase regulates Th1 and Th17 cell differentiation by controlling Akt-mTOR signaling. bioRxiv. 2024:2024.01.08.574595.
35. Lee B, Park SJ, Lee S, Park SE, Lee E, Song JJ, et al. Identification of the Antidepressant Vilazodone as an Inhibitor of Inositol Polyphosphate Multikinase by Structure-Based Drug Repositioning. Mol Cells. 2020;43(3):222–7.
36. Jones NP, Peak J, Brader S, Eccles SA, Katan M. PLCgamma1 is essential for early events in integrin signalling required for cell motility. J Cell Sci. 2005;118(Pt 12):2695–706.
37. Rodriguez R, Matsuda M, Perisic O, Bravo J, Paul A, Jones NP, et al. Tyrosine residues in phospholipase Cgamma 2 essential for the enzyme function in B-cell signaling. J Biol Chem. 2001;276(51):47982–92.
38. Wendt ER, Ferry H, Greaves DR, Keshav S. Ratiometric analysis of fura red by flow cytometry: a technique for monitoring intracellular calcium flux in primary cell subsets. PLoS ONE. 2015;10(3):e0119532.
39. Tiegs G, Hentschel J, Wendel A. A T cell-dependent experimental liver injury in mice inducible by concanavalin A. J Clin Invest. 1992;90(1):196–203.
40. Floreani A, Restrepo-Jiménez P, Secchi MF, De Martin S, Leung PSC, Krawitt E, et al. Etiopathogenesis of autoimmune hepatitis. J Autoimmun. 2018;95:133–43.
41. Christen U. Animal models of autoimmune hepatitis. Biochim Biophys Acta Mol Basis Dis. 2019;1865(5):970–81.
42. Mizuhara H, O'Neill E, Seki N, Ogawa T, Kusunoki C, Otsuka K, et al. T cell activation-associated hepatic injury: mediation by tumor necrosis factors and protection by interleukin 6. J Exp Med. 1994;179(5):1529–37.
43. Nagata T, McKinley L, Peschon JJ, Alcorn JF, Aujla SJ, Kolls JK. Requirement of IL-17RA in Con A induced hepatitis and negative regulation of IL-17 production in mouse T cells. J Immunol. 2008;181(11):7473–9.
44. Lv K, Zhang Y, Zhang M, Zhong M, Suo Q. Galectin-9 ameliorates Con A-induced hepatitis by inducing CD4(+)CD25(low/int) effector T-Cell apoptosis and increasing regulatory T cell number. PLoS ONE. 2012;7(10):e48379.
45. Palacios R, Concanavalin. A triggers T lymphocytes by directly interacting with their receptors for activation. J Immunol. 1982;128(1):337–42.
46. Richard S, Yu D, Blumer KJ, Hausladen D, Olszowy MW, Connelly PA, et al. Association of p62, a multifunctional SH2- and SH3-domain-binding protein, with src family tyrosine kinases, Grb2, and phospholipase C gamma-1. Mol Cell Biol. 1995;15(1):186–97.
47. Choi J-M, Ahn M-H, Chae W-J, Jung Y-G, Park J-C, Song H-M, et al. Intranasal delivery of the cytoplasmic domain of CTLA-4 using a novel protein transduction domain prevents allergic inflammation. Nat Med. 2006;12(5):574–9.
48. Gresset A, Hicks SN, Harden TK, Sondek J. Mechanism of phosphorylation-induced activation of phospholipase C-gamma isozymes. J Biol Chem. 2010;285(46):35836–47.
49. Braiman A, Barda-Saad M, Sommers CL, Samelson LE. Recruitment and activation of PLCgamma1 in T cells: a new insight into old domains. Embo j. 2006;25(4):774–84.
50. Yokoyama JS, Wang Y, Schork AJ, Thompson WK, Karch CM, Cruchaga C, et al. Association Between Genetic Traits for Immune-Mediated Diseases and Alzheimer Disease. JAMA Neurol. 2016;73(6):691–7.
51. O'Donnell S, Borowski K, Espin-Garcia O, Milgrom R, Kabakchiev B, Stempak J, et al. The Unsolved Link of Genetic Markers and Crohn's Disease Progression: A North American Cohort Experience. Inflamm Bowel Dis. 2019;25(9):1541–9.

Publisher's note